

# Spectroscopic studies of solids using correlation photoacoustic spectroscopy (CPAS)

Andreas Mandelis and James T Dodgson

Photoacoustics and Photothermal Sciences Laboratory, Department of Mechanical Engineering, University of Toronto, Toronto, Ontario M5S 1A4, Canada

Received 12 June 1985

**Abstract.** Cross-correlation photoacoustic spectroscopy (CPAS) of condensed matter carries spectroscopic information related to the optical absorption coefficient of solids in both signal magnitude and time delay channels. A one-dimensional theoretical model is presented in which the cross-correlation photoacoustic response to pseudo-random-binary-sequence (PRBS) optical excitation is evaluated for systems of variable optical absorption coefficients. The model is further compared to CPAS data from powders of  $\text{Ho}_2\text{O}_3$  in the visible spectral range.

## 1. Introduction

Correlation photoacoustic spectroscopy (CPAS) is a relatively new technique, first reported in 1980 (Kato *et al* 1980). In that work and subsequent publications (Sugitani *et al* 1982, Kirkbright *et al* 1983a, b, Kirkbright and Miller 1983) the main emphasis was given to establishing the potential of CPAS as a technique capable of performing depth profiling and thermal wave imaging in layered solids in a qualitative fashion. The spectroscopic abilities of CPAS were also investigated qualitatively simultaneously with its depth-profiling character (Kato *et al* 1980, Sugitani *et al* 1982, Kirkbright *et al* 1984a, b, Uejima *et al* 1985). Correlation photoacoustic spectroscopy was thus shown to be able to produce spectra of solids when the wavelength of the exciting radiation was scanned.

The only theoretical attempt to quantify the depth-profiling capability of CPAS up to now was made by Uejima *et al* (1984). The results of the thermal model proposed by these authors were empirically fitted into experimental data from the cross-correlation peak time delay against sample thickness plot and the agreement was found to be satisfactory.

The spectroscopic character of CPAS has not been investigated systematically and/or quantitatively. The experimentally obtained photoacoustic spectra, however, are expected to be subject to limitations such as photoacoustic saturation (Rosencwaig and Gersho 1976) and microphone frequency response (Mandelis and Royce 1980). Sugitani *et al* (1982) showed that the cross-correlation function of the input and the resultant output function of a randomly excited system is equal to the impulse-response function of the linear system. It is, therefore, expected that the equivalent-pulse duration of a pseudo-random binary sequence (PRBS) optical excitation will affect the cross-correlation PAS response of the system in both magnitude and time delay (Mandelis and

Royce 1979). In this paper we present a theoretical study of the optical absorption coefficient-dependent CPAS signal and we compare the results of our model to experimental spectroscopic data from holmium oxide ( $\text{Ho}_2\text{O}_3$ ) powders. We thus determine under what conditions CPAS can qualify as a quantitative spectroscopic technique, capable of measuring optical absorption coefficients unambiguously.

## 2. Theoretical pseudo-random response of the microphone–gas photoacoustic cell

A one-dimensional model similar to one employed previously (Mandelis and Royce 1979, 1980) is assumed (figure 1). Optical, acoustic and thermal processes occur in a microphone–gas-coupled photoacoustic cell excited by a PRBS optical pulse train (Sugitani *et al* 1982). The absorbing solid of thickness  $l$ , having an optical absorption coefficient  $\beta(\lambda)$ , is supported by an assumed optically transparent backing. The cell, of length  $L$ , contains an optically transparent gas, such as air and the optical pulse train enters the cell through a non-absorbing window. The light pulse irradiance is  $I_0$  and the non-radiative de-excitation processes following light absorption in the solid are taken to be instantaneous. For small enough cells the pressure inside the sample chamber (i.e. the photoacoustic signal) is assumed to be uniform throughout the cell and to exhibit no delays due to the finite velocity of sound.

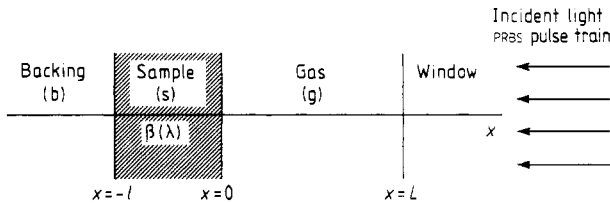


Figure 1. One-dimensional geometry of CPAS sample cell for theoretical model.

Under these conditions, the thermal diffusion equations for each of the regions of the cell can be written as follows:

$$\frac{\partial^2}{\partial x^2} T_g(x, t) - \frac{1}{\alpha_g} \frac{\partial}{\partial t} T_g(x, t) = 0 \quad 0 \leq x \leq L \quad (1a)$$

$$\frac{\partial^2}{\partial x^2} T_s(x, t) - \frac{1}{\alpha_s} \frac{\partial}{\partial t} T_s(x, t) = -\frac{\eta \beta I_0}{k_s} \exp(\beta x) F(t) \quad -l \leq x \leq 0 \quad (1b)$$

$$\frac{\partial^2}{\partial x^2} T_b(x, t) - \frac{1}{\alpha_b} \frac{\partial}{\partial t} T_b(x, t) = 0 \quad x \leq -l. \quad (1c)$$

In equations 1(a)–(c),  $T_i(x, t)$  are the temperatures of the gas ( $i = g$ ), sample ( $i = s$ ) and backing ( $i = b$ ), respectively. The symbols  $\alpha_i$ ,  $\eta$ ,  $k_s$  denote thermal diffusivity of component ( $i$ ), quantum efficiency of the non-radiative processes in the solid and thermal conductivity of the solid,  $F(t)$  is the PRBS light modulation wavetrain (figure 2). Equations 1(a)–(c) are coupled by the boundary conditions of temperature and heat flux continuity at the interfaces  $x = 0, -l$ . In the time domain, solutions can be obtained in the Laplace space  $s$  by taking the Laplace transforms of equations (1). The temperature profile in

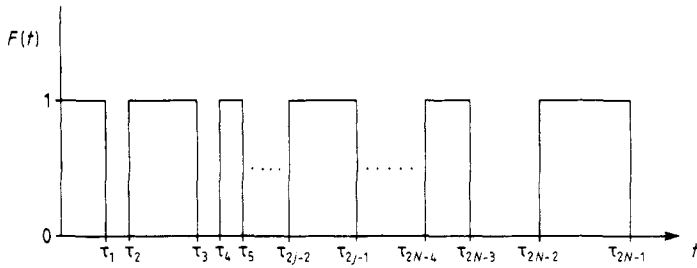


**Figure 2.** Theoretical normalised pseudo-random binary sequence (PRBS) optical excitation wavetrain incident on the sample. Total number of pulses in sequence is  $N = 127$ ; duration of the  $j$ th pulse is  $\Delta \tau_j = \tau_{2j-1} - \tau_{2j-2}$ .

the gas chamber  $T_g(x, t)$  can thus be shown to have the following Laplace transform:

$$\hat{T}_g(x, s) = A(s) \left\{ [(r - 1)(b_{bs} + 1) \exp(a_s l) - (r + 1)(b_{bs} - 1) \exp(-a_s l) + 2(b_{bs} - r) \exp(-\beta l)] / [(b_{gs} + 1)(b_{bs} + 1) \exp(a_s l) - (b_{gs} - 1)(b_{bs} - 1) \exp(-a_s l)] \right\} \exp(-a_g x) \tag{2}$$

where

$$A(s) \equiv \left( \frac{\eta \beta I_0 \alpha_s}{k_s} \right) \left( \frac{\hat{F}(s)}{\alpha_s \beta^2 - s} \right) \tag{3}$$

$$r \equiv \beta / a_s \quad b_{ij} \equiv k_i a_i / k_j a_j \quad a_i \equiv (s / \alpha_i)^{1/2} \tag{4}$$

and  $\hat{F}(s)$  is the Laplace transform of the PRBS optical wavetrain. Equation (2) is a special case of a previously derived more general expression (Mandelis and Royce 1979), valid in the limit of a thermally thick sample chamber, i.e. for

$$a_g \gg L^{-1}$$

which translates to detection times such that

$$t \ll L^2 / \alpha_g \equiv \tau_D^g. \tag{5}$$

$\tau_D^g$  is the characteristic diffusion time required for thermal energy to cross the distance between the sample surface ( $x = 0$ ) and the cell window ( $x = L$ ).

The Laplace transform of the incremental pressure rise in the sample cell due to the gas temperature rise is given by (Mandelis and Royce 1979):

$$\Delta \hat{P}(s) = \frac{P_0}{T_0 L} \int_0^L \hat{T}_g(x, s) dx \tag{6}$$

where  $T_0$  is the ambient temperature. In deriving equation (6) the ideal gas law was assumed. The result of the integration over the cell length is

$$\Delta \hat{P}(s) = \left( \frac{P_0}{T_0 L \alpha_g} \right) A(s) \times \left( \frac{(r - 1)(b_{bs} + 1) \exp(a_s l) - (r + 1)(b_{bs} - 1) \exp(-a_s l) + 2(b_{bs} - r) \exp(-\beta l)}{(b_{gs} + 1)(b_{bs} + 1) \exp(a_s l) - (b_{gs} - 1)(b_{bs} - 1) \exp(-a_s l)} \right). \tag{7}$$

Equation (7) can be inverted explicitly to yield  $\Delta P(t)$  only in special cases. Experimentally, a very important special case is that of a thermally thick sample, for which  $\exp(-a_s l) \approx 0$ . This is frequently the limit of a physically thick sample with poor thermal conduction properties (i.e. low  $\alpha_s$ ). In the time domain, this limit can be achieved for any sample, provided the experiment is performed within a maximum time  $t_{\max}$  such that

$$t_{\max} \ll l^2/\alpha_s \equiv \tau_D^s \quad (8)$$

where ' $\ll$ ' means 'at least one order of magnitude', and  $\tau_D^s$  is the thermal diffusion time to the back of the sample. Under condition (8), equation (7) simplifies to

$$\Delta \hat{P}(s) = \frac{P_0 A(s)}{T_0 L a_g(s)} [r(s) - 1]. \quad (9)$$

In order to relate the theoretical expression (9) to experimental data from cross-correlation studies, the frequency response of the photoacoustic transducer (microphone) must be taken into account. It can be shown (Mandelis and Royce 1980) that the Laplace transforms of the microphone voltage response,  $\Delta \hat{V}(s)$ , and the PAS cell pressure,  $\Delta \hat{P}(s)$ , are related through

$$\Delta \hat{V}(s) = \frac{A_0 E}{\omega_m^2 m} \left( \frac{\tau_{RC} s}{1 + \tau_{RC} s} \right) \Delta \hat{P}(s) \quad (10)$$

in the linear regime of the microphone frequency response curve (i.e. well below resonance). In equation (10),  $A_0$  is the area of the microphone diaphragm,  $E$  is the microphone polarisation voltage,  $m$  is the mass of the diaphragm,  $\omega_m$  is the undamped natural angular frequency of the transducer, and  $\tau_{RC}$  is the RC time constant of the resistive/capacitive electrical circuit of the microphone. Equation (10), when taken for times *large* compared to  $\tau_{RC}$  ( $\approx 30$  ms for the 1/8 in B & K condenser microphone model 4138) becomes

$$\Delta \hat{V}(s) \approx G s \Delta \hat{P}(s) \quad (11)$$

with

$$G \equiv E(A_0 \tau_{RC} / \omega_m^2 m) = \text{constant}. \quad (12)$$

Using equations (9) and (11), the integral form of the inverted time-domain response is (Spiegel 1965)

$$\Delta V(t; \beta) = G [Y(\beta) / \tau_\beta^{1/2}] \left[ \left( \frac{\tau_\beta}{\pi} \right)^{1/2} \int_0^t \frac{F(u) du}{(t-u)^{1/2}} - \int_0^t F(u) \exp[(t-u)/\tau_\beta] \operatorname{erfc}[(t-u)/\tau_\beta]^{1/2} du \right] \quad (13)$$

where

$$Y(\beta) \equiv P_0 I_0 \eta \beta \alpha_s \alpha_g^{1/2} / T_0 L k_s \quad (14)$$

and

$$\tau_\beta \equiv 1/\beta^2 \alpha_s. \quad (15)$$

Figure 2 shows that the PRBS optical wavetrain can be expressed symbolically in the form:

$$F(t) = \sum_{j=1}^N f_j(t)$$

$$f_j(t) = \begin{cases} 1 & \tau_{j-1} < t < \tau_j \\ 0 & \tau_j < t < \tau_{j+1} \end{cases} \quad (16)$$

where  $N$  square optical pulses were assumed, the duration of the  $j$ th pulse being variable and given by

$$\Delta\tau_j = \tau_{2j-1} - \tau_{2j-2} \quad (17)$$

with  $\tau_0 \equiv 0$ . The pseudo-periodic wavetrain repeats its random sequence after a time interval

$$T = \tau_{2N-1}. \quad (18)$$

The intensity (height) of each pulse in figure 2 is unity, to be multiplied by  $I_0$ , which is incorporated within  $Y(\beta)$  as a factor common to all pulses.

Introducing equation (16) into (13), and carrying out the integrations, yields the following expression for the photoacoustic response to the PRBS excitation:

$$V(t; \tau_\beta) = GY(\beta)\tau_\beta \begin{cases} \sum_{j=1}^{N-1} \left[ Z\left(\frac{t-\tau_{2j-1}}{\tau_\beta}\right) - Z\left(\frac{t-\tau_{2j-2}}{\tau_\beta}\right) \right] \\ + Z(0) - Z\left(\frac{t-\tau_{2N-2}}{\tau_\beta}\right) & \tau_{2N-2} \leq t \leq \tau_{2N-1} \\ \sum_{j=1}^N \left[ Z\left(\frac{t-\tau_{2j-1}}{\tau_\beta}\right) - Z\left(\frac{t-\tau_{2j-2}}{\tau_\beta}\right) \right] & t \geq \tau_{2N-1} \end{cases} \quad (19)$$

where

$$Z(x) \equiv e^x \operatorname{erfc}(\sqrt{x}) \quad (20a)$$

with

$$\sum_{j=1}^{N-1} [ ] = 0 \quad \text{for } N = 1. \quad (20b)$$

It is easy to show that the expressions valid for  $\tau_{2N-2} \leq t \leq \tau_{2N-1}$  and for  $t \geq \tau_{2N-1}$  in equation (19) coincide for  $t = \tau_{2N-1}$ , as expected. The characteristic time  $\tau_\beta$  of the solid, defined in equation (15) corresponds to the thermal transit time from a depth in the solid equal to the optical absorption length,  $[\beta(\lambda)]^{-1}$ , at a given wavelength (Mandelis and Royce 1979). It ought to be emphasised that the expression for the photoacoustic response to a pseudo-random optical excitation, equation (19), is generally valid for any values of the optical absorption coefficient  $\beta$ , as long as the sample and the cell are thermally thick (Rosencwaig and Gersho 1976).

**3. Signal cross-correlation theory applied to PAS**

The cross-correlation technique is a stochastic process based on the premise that one variable  $x(t)$  can influence the future value of another variable  $y(t)$ . In the particular application of CPAS

$$x(t) = F(t) \tag{21}$$

and

$$y(t) = V(t; \tau_\beta). \tag{22}$$

The cross-correlation function of these two time-varying signals is denoted by  $R_{FV}$  and is defined by the relationship (Godfrey 1980)

$$R_{FV}(\tau; \tau_\beta) = \lim_{T \rightarrow \infty} \frac{1}{2T} \int_{-T}^T F(t)V(t + \tau; \tau_\beta) dt. \tag{23}$$

$T$  is the pseudo-period given in our model by equation (18) and both  $F(t)$  and  $V(t; \tau_\beta)$  are assumed to be zero-mean, weakly stationary, ergodic random signals. Some of the most important properties of  $R_{FV}$  have been discussed by Godfrey (1980). In order to perform cross-correlation calculations numerically using a computer, certain modifications must be made to equation (23):

$$R_{FV}(\tau_r; \tau_\beta) = \frac{1}{(n - r)} \sum_{k=1}^{n-r} F_k V_{k+r} \tag{24}$$

where

$$\tau_r = r\Delta t \tag{25}$$

$$\Delta t = 1/SR \tag{26}$$

and

$$r = 0, 1, 2, \dots, Q.$$

SR is the sampling rate used in the data acquisition,  $n$  is the number of samples taken of data pairs,  $r$  is an integer greater than or equal to 0, and  $Q$  is the number of cross-correlations calculated. For a good estimate of the cross-correlation function,  $Q$  should be less than 10% of  $n$ . If  $F(t)$  is a genuinely random function of time (e.g. white noise), then its autocorrelation function is proportional to the Dirac delta function. In the microphone-gas coupled PAS, the presence of acoustic noise in the cell in addition to the PAS signal results in a composite response

$$W(t; \tau_\beta) = V(t; \tau_\beta) + n(t) \tag{27}$$

so that (Godfrey 1980)

$$R_{FW}(\tau; \tau_\beta) = R_{FV}(\tau; \tau_\beta) + R_{Fn}(\tau). \tag{28}$$

As  $F(t)$  and  $n(t)$  are statistically independent from each other, in the limit  $T \rightarrow \infty$  it is expected that  $R_{Fn} \rightarrow 0$ , i.e.

$$R_{FW}(\tau; \tau_\beta) = R_{FV}(\tau; \tau_\beta) \quad T \rightarrow \infty. \tag{29}$$

The problem of generating a truly random noise excitation was overcome by generating a pseudo-random optical wavetrain, which has the same type of autocorrelation function as white noise (i.e. a Dirac-type impulse), but which is repeated with a pseudo-period  $T$ . The PRBS was chosen for this work as a pseudo-random excitation based on a maximum length linear shift register sequence (M series), the light modulation sequence given by (Golomb 1967)

$$N = 2^n - 1 \quad (30)$$

with  $n = 7$  (Sugitani *et al* 1982), and  $N = 127$  representing the length of the pseudo-period

$$T = Nt_0. \quad (31)$$

$t_0$  is the minimum time interval in the sequence. All optical pulses in the sequence are integral multiples of  $t_0$ .

#### 4. Spectroscopic apparatus and materials

A schematic diagram of the experimental apparatus is shown in figure 3. Light sources used for optical excitation of the samples were a 1 mW He-Ne laser and a 1000 W xenon lamp (Oriel model 6141 with photo-feedback control). For CPAS measurements, a special PRBS light chopper was made based on equation (30) and similar to the one used by Sugitani *et al* (1982). The chopper blade, machined out of a  $\frac{1}{8}$  in thick black anodised aluminum plate, was fitted to the chopper blade holder of an AMKO model OC 4000 mechanical chopper. This allowed controllability of the rotation frequency of the PRBS chopper via calibration of the motor drive digital display through an LED located at the base of the chopper blade holder. The quartz beamsplitter was used to direct a fraction of the radiation to the UV-enhanced photodiode (Silicon Detector Corp. model SD-100-13-13-022), whose signal, when amplified by a Keithley model 427 current amplifier, was used as the  $F(t)$  in equation (23). The output of the photoacoustic cell, EG & G Princeton Applied Research model 6003 and matching preamplifier model 6005, was further

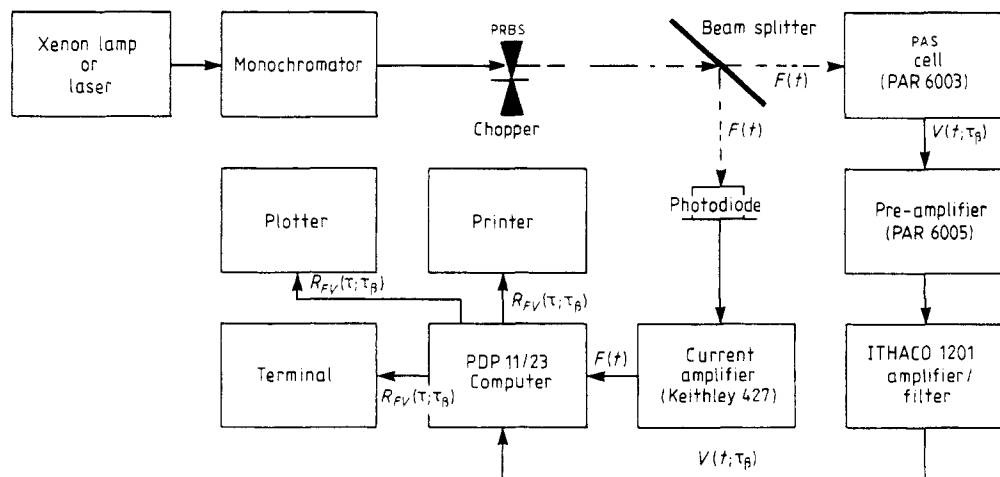


Figure 3. CPAS microphone-gas-coupled experimental apparatus.

filtered through an Ithaco model 1201 low noise preamplifier/bandpass filter. A DEC PDP 11/23 computer was interfaced to the experimental set up with the aid of a data translation AD converter (model DT 3392). This is a 12 bit converter operational at frequencies up to 125 kHz for two channels. Cross correlations were performed digitally, based on equations (24)–(29).

The materials used for spectroscopic investigations were carbon black powder (Xerox toner) as a reference, and  $\text{Ho}_2\text{O}_3$  powder (Aldrich Chemical Co., 99.9% purity). This rare earth oxide was chosen for the strong and sharp transition peaks it exhibits in its visible absorption spectrum, as a means of detecting the variation of the absorption coefficient (Schoonover *et al* 1984); it was also used in a powdered form due to the high surface-to-volume ratio of the particulates, which enhanced the CPAS signal-to-noise ratio (SNR) considerably. The spectral region chosen for  $\text{Ho}_2\text{O}_3$  CPAS was between 420–515 nm, as the  $\text{Ho}^{3+}$  ion exhibits a strong broad absorption band for the 8 nm resolution of our experiments. This broad band, in fact, consists of spectral peaks given the assignments  $^5\text{F}_2$  (474 nm),  $^3\text{K}_8$  (464 nm),  $^5\text{G}_6$  (457 nm), and  $^5\text{G}_5$  (450 nm). Of the four peaks, all of which were resolvable with our apparatus at 2 nm resolution, the first peak appears as a broad shoulder and the last three are broadened to form the observed broad band at the 8 nm resolution level.

## 5. Experimental and results

For reasons of comparison between experiment and CPAS theory, the thermal diffusivity and optical absorption spectrum of  $\text{Ho}_2\text{O}_3$  were measured using a conventional frequency-domain photoacoustic (F-D PAS) spectrometer described elsewhere (Mandelis *et al* 1984). In order to use the well known method of thermal diffusivity calculation from the slope of the PAS phase against frequency curve (Adams and Kirkbright 1977a, b), a thin layer of  $\text{Ho}_2\text{O}_3$  powder ( $39 \pm 10 \mu\text{m}$ ) was deposited on a carbon black backing and irradiated with 515 nm light, i.e. in a spectral region where the optical absorption coefficient has a minimum (Schoonover *et al* 1984). In this manner the  $\text{Ho}_2\text{O}_3$  thin layer was expected (and later proven) to be optically transparent ( $\beta l \approx 2 \times 10^{-3}$ ). Transparency was verified by examining two PAS spectra spanning the 420–520 nm region at 50 and 100 Hz. Comparison of the ratio  $R_p$  of the two peak signals at 450 nm and that of the two valleys  $R_v$  at 515 nm showed that the valley signals contained a strong component from the underlying carbon black:

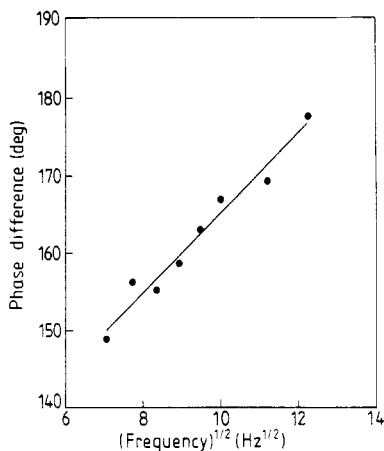
$$R_p(50 \text{ Hz}/100 \text{ Hz}) = 2.2 < R_v(50 \text{ Hz}/100 \text{ Hz}) = 4.67.$$

Figure 4 shows the F-D PAS phase data obtained from the  $\text{Ho}_2\text{O}_3$  thin layer for 515 nm illumination at chopping frequencies between  $f = 50$  and 200 Hz. Phase differences  $\Delta\Psi$  were measured with the sample in place and with an empty holder. The thermal diffusivity of  $\text{Ho}_2\text{O}_3$  was calculated, assuming the powder to be transparent and using the equation (Adams and Kirkbright 1976, Mandelis *et al* 1979)

$$\Delta\Psi = [(\pi/\alpha_s)^{1/2} l] f^{1/2}. \quad (32)$$

A least-squares fit to the data in figure 4 gave a slope value from which the thermal diffusivity was found to be

$$\alpha_{\text{Ho}_2\text{O}_3} = 0.0059 \pm 0.0004 \text{ cm}^2 \text{ s}^{-1}. \quad (33)$$



**Figure 4.** Least-squares fit to the plot of F-D PAS phase lag against the square root of modulation frequency for  $39 \pm 10 \mu\text{m}$  thick  $\text{Ho}_2\text{O}_3$  powders on black backing. Irradiation wavelength: 515 nm.

To our knowledge, this is the first ever calculation of the thermal diffusivity of  $\text{Ho}_2\text{O}_3$ . Comparisons can be made, however, to other rare earth oxides. The literature values for yttrium oxide ( $\text{Y}_2\text{O}_3$ ), samarium oxide ( $\text{Sm}_2\text{O}_3$ ), erbium oxide ( $\text{Er}_2\text{O}_3$ ), and lutetium oxide ( $\text{Lu}_2\text{O}_3$ ) are (Gemlin 1974), respectively: 0.015, 0.0049, 0.012 and 0.014  $\text{cm}^2 \text{s}^{-1}$  at 20 °C. The determined value for  $\text{Ho}_2\text{O}_3$  certainly fits into this range and was subsequently used in our theoretical calculations.

The values for the optical absorption coefficient were determined by normalising the F-D PAS holmium oxide spectrum to a single value for  $\beta(446 \text{ nm})$  calculated from a recent work by Carlson and Hodul (1982). From that study, the value of  $\beta$  at 446 nm can be found to be 22.44  $\text{cm}^{-1}$  with 2 nm resolution. The normalised optical absorption spectrum of  $\text{Ho}_2\text{O}_3$  powder in this work (8 nm resolution) is shown in figure 5.

Figure 6 shows the CPAS visible spectrum of the Xerox toner normalised by the xenon

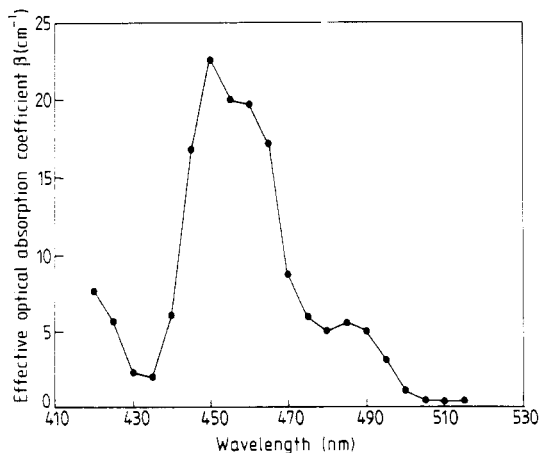


**Figure 5.** Effective optical absorption spectrum of  $\text{Ho}_2\text{O}_3$  powders determined photoacoustically with 8 nm resolution, using data from Carlson and Hodul (1982).

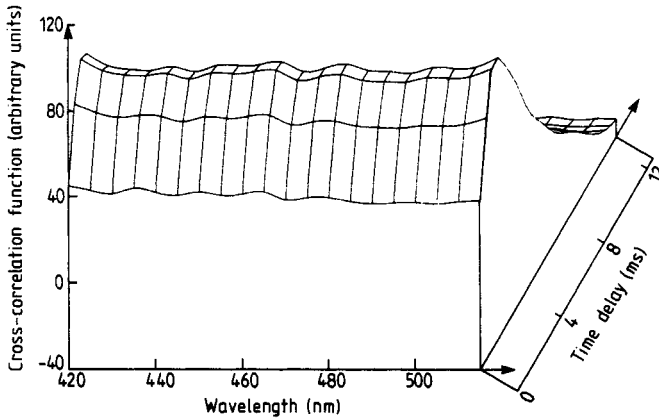
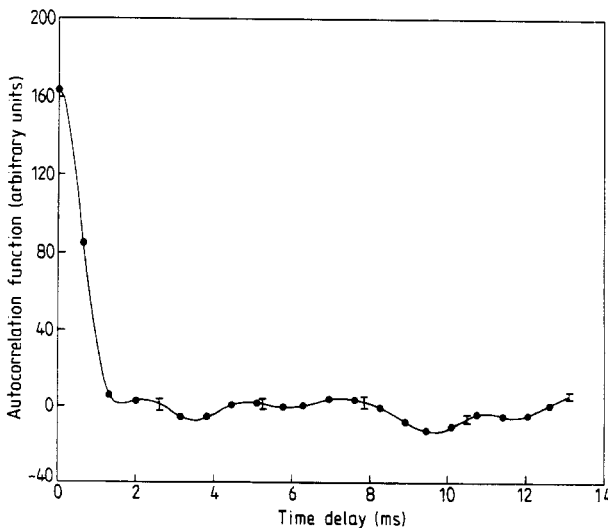


**Figure 6.** Cross-correlation function (CPAS spectrum) of normalised signal from Xerox toner. Chopper speed:  $6 \text{ rev s}^{-1}$ ; pre-amp filter bandpass: 30–10 kHz.

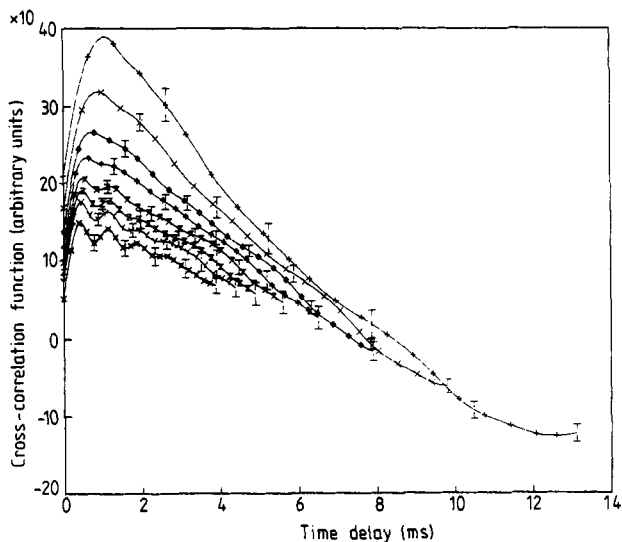
lamp, beamsplitter and photodiode optical transfer functions, with the cross-correlation time delay as a parameter. The spectrum exhibits photoacoustic saturation, as expected from optically opaque and thermally thick solids (Rosencwaig and Gersho 1976).

Figure 7 shows the autocorrelation of the PRBS chopper under He–Ne laser excitation. The autocorrelation function peaks at  $\tau = 0 \text{ s}$  and becomes negative at  $\tau = 1.35 \text{ ms}$  at a rotational chopper frequency of 6 Hz. The time oscillatory behaviour of this function is typical of autocorrelations corresponding to band-limited white noise spectra (Crandall and Mark 1963). The autocorrelation function’s characteristic time of 1.35 ms for sign change is in very good agreement with the smallest time unit  $t_0 = 1.31 \text{ ms}$  of the PRBS chopper at 6 Hz, to which it is expected to be theoretically equal (Godfrey 1980).

Figure 8 shows the 632.8 nm CPAS signal for the Xerox toner at various PRBS chopper blade speeds. This figure indicates a decrease in the magnitude of the cross-correlation



**Figure 7.** Autocorrelation function of the PRBS chopper.



**Figure 8.** CPAS signals from Xerox toner at 632.8 nm and various PRBS chopper speeds in  $\text{rev s}^{-1}$ : +, 6;  $\times$ , 8;  $\diamond$ , 10;  $\uparrow$ , 12;  $\times$ , 14; Z, 16; Y, 18;  $\boxtimes$ , 20.

function with increasing rotational frequency, as well as a decrease in the peak time delay. Similar trends were previously observed by Sugitani and Uejima (1984). Comparing values, the peak time delay observed by these authors was 0.5 ms at  $12 \text{ rev s}^{-1}$  compared to 0.63 ms obtained in our experiments. This small difference can be easily attributed to the different experimental set-ups, and primarily to different microphones and signal processing devices (our computer/mathematical cross correlation compared with their time-delay-unit/analog cross correlation).

The holmium oxide powder CPAS spectrum is shown in figure 9 with the delay time as a parameter. The three-dimensional surface shows the expected strong absorption

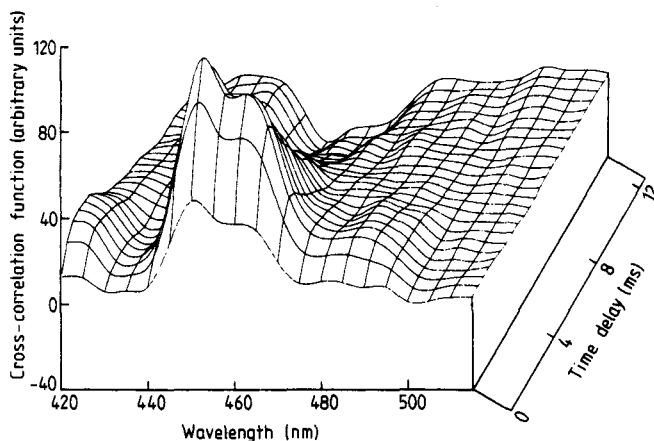


**Figure 9.** Cross-correlation function (CPAS spectrum) of normalised signal from  $\text{Ho}_2\text{O}_3$  powder. Chopper speed:  $6 \text{ rev s}^{-1}$ ; pre-amp filter bandpass: 30–10 kHz.

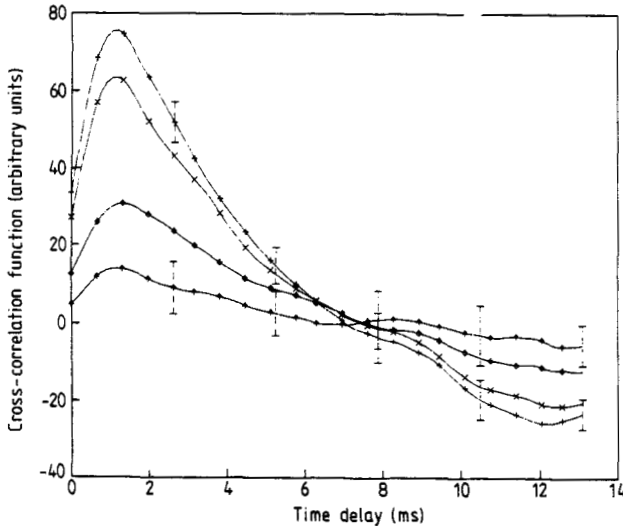


Figure 10. Cross-correlation function of  $\text{HO}_2\text{O}_3$  at various wavelengths: +, 450 nm ( $\beta \approx 22.4 \text{ cm}^{-1}$ );  $\times$ , 446 nm ( $\beta \approx 16.6 \text{ cm}^{-1}$ );  $\diamond$ , 442 nm ( $\beta \approx 6.5 \text{ cm}^{-1}$ );  $\uparrow$ , 438 nm ( $\beta \approx 5.5 \text{ cm}^{-1}$ ).

between 445 and 470 nm flanked by relatively transparent regions. In the strongly absorbing region and behind the frontal peaks, a depression mirroring the peak intensities can be seen. We believe this depression to be due to the microphone 'flyback' effect, which has been observed in the impulse-response studies of Cox and Coleman (1981). These authors found that in impulse-response PAS, the signal depression below the baseline noise level after the end of the optical pulse was due to the fact that the microphone would overshoot the actual pressure in the cell because of the rapid change in pressure

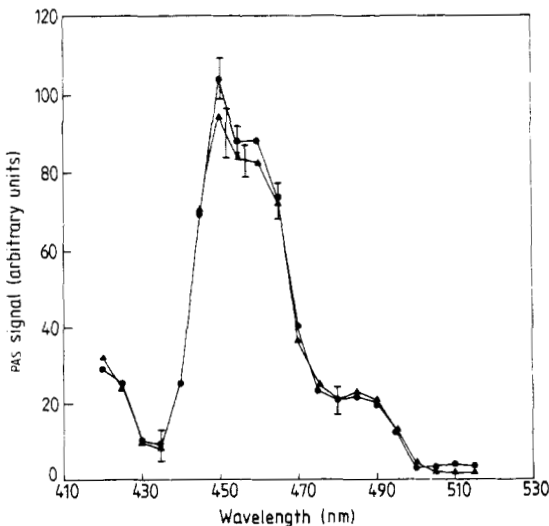


Figure 11. F-D PAS ( $\triangle$ ) amplitude at 50 Hz and CPAS ( $\circ$ ) magnitude at  $6 \text{ rev s}^{-1}$ . Both curves were artificially matched at 440 nm.

with strongly absorbing samples. This effect can be ultimately traced to the mechanical inertia of the microphone diaphragm itself.

The CPAS function for  $\text{Ho}_2\text{O}_3$  at various absorption coefficient values between 436 and 450 nm is shown in figure 10. In this spectral region the powder changes from optically transparent to opaque. With the value for  $\alpha_{\text{Ho}_2\text{O}_3}$  given by equation (33) and a sample thickness of approximately 1.6 mm, the sample was found to be thermally thick at all times during a cross-correlation experiment: the thermal transit time through the sample thickness was calculated to be 4.12 s, much greater than the longest light pulse duration of 9.2 ms. In figure 10 the CPAS magnitude decreases with decreasing  $\beta$ .

Figure 11 shows a comparison between a F-D PAS spectrum of  $\text{Ho}_2\text{O}_3$  (photoacoustic amplitude) taken with lock-in detection at 50 Hz and the CPAS average magnitude of 20 cross-correlations, at the peak time delay taken at 6 rev  $\text{s}^{-1}$ . The detailed agreement of the spectral features across the transition band confirms that the peak magnitude of the CPAS gives optical absorption information equivalent to the conventional F-D PAS.

## 6. Discussion

The optical absorption coefficient values calculated for  $\text{Ho}_2\text{O}_3$  and shown in figure 5 span two orders of magnitude ( $0.38\text{--}22.44 \text{ cm}^{-1}$ ) and can thus provide a broad range for testing the spectroscopic capability of CPAS. For comparison with our theory, it would have been more desirable to use single crystalline materials, which could be assumed to be truly one-dimensional with respect to their optical and thermal properties. Preliminary tests with CdS single crystals unfortunately exhibited SNRs too low for the quantitative purposes of the present work, even at super-band-gap excitations. Spectroscopic data of hydrated  $\text{Ho}_2\text{O}_3$  pastes showed no difference from the powdered samples and subsequently the powders were treated as one-dimensional samples.

Tilgner (1981) has raised some valid objections, however, as to the nature of the photoacoustic spectra of powders and their (often implicitly assumed) correspondence to optical absorption/transmission spectra. In principle, the F-D PAS scales with the optical absorption coefficient when the thermal diffusion length,  $\mu_s = (2\alpha_s/\omega)^{1/2}$ , is smaller than the optical absorption depth,  $\mu_\beta = \beta^{-1}$ , according to Rosencwaig and Gersho (1976). Hass *et al* (1959) evaluated the optical properties of evaporated rare-earth oxide films, such as  $\text{Nd}_2\text{O}_3$  and  $\text{La}_2\text{O}_3$ , in the wavelength region between 0.22 and 2  $\mu\text{m}$ . From the measured extinction coefficient (i.e. the imaginary part of the refractive index), the optical absorption coefficients for  $\text{Nd}_2\text{O}_3$  and  $\text{La}_2\text{O}_3$  can be calculated at 400 nm:

$$\beta_{\text{Nd}_2\text{O}_3}(400 \text{ nm}) \approx 6.3 \times 10^3 \text{ cm}^{-1}$$

$$\beta_{\text{La}_2\text{O}_3}(400 \text{ nm}) \approx 3 \times 10^3 \text{ cm}^{-1}.$$

These values imply optical absorption depths of 1.6 and 3.3  $\mu\text{m}$ , respectively. Tilgner (1981) has pointed out that the condition  $\mu_s < \mu_\beta$  can only be satisfied for modulation frequencies in the megahertz range and higher for rare earth oxides. At lower frequencies rare-earth oxide powders should normally be saturated photoacoustically. Tilgner attributed the apparent spectral features exhibited by these oxides under the PAS probe to the effect of wavelength-dependent strong surface reflections, with corroborating evidence from diffuse reflectance measurements on  $\text{Nd}_2\text{O}_3$  and  $\text{Ho}_2\text{O}_3$ . The net effect of Tilgner's work is that the PAS spectrum from  $\text{Ho}_2\text{O}_3$  essentially duplicates the diffuse

reflectance spectrum from this material, which does contain spectral information about the sample. Our CPAS results and those of Carlson and Hodul (1982) also show that  $\text{Ho}_2\text{O}_3$  powders behave as a photoacoustically non-saturated solid with an *effective* variable optical absorption coefficient throughout the spectral region of interest according to figure 5, in agreement with the assumptions of the theory presented in § 2 above.

The experimental CPAS data were further compared to predictions from our model. Utilising the values for  $\alpha_{\text{Ho}_2\text{O}_3}$  and  $\beta_{\text{Ho}_2\text{O}_3}(\lambda)$  found in our experiments, the cross-correlation function was calculated for a particular  $F(t)$  input and an output  $V(t; \tau_\beta)$  predicted from the theory, equation (19). In order to model our experiments as closely as possible, the PRBS sequence that was used in the experiments was also modelled as  $F(t)$  in the theoretical analysis. The PRBS was broken down into 1270 discrete time intervals, just as in the experiments, and the resulting theoretical microphone response was cross correlated numerically with the PRBS optical excitation wavetrain. Each series of calculations was made of a duration equal to one rotation of the chopper blade, and was repeated 20 times at different starting positions of the wavetrain in order to model

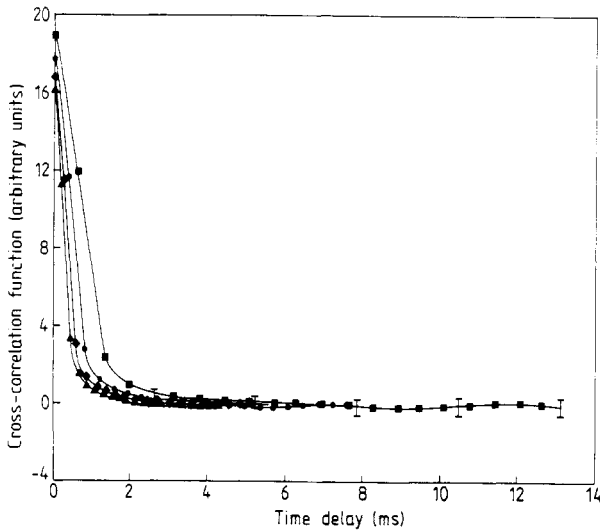


**Figure 12.** Theoretical cross-correlation function for optically opaque solids with the chopper speed as a parameter: ■, 6 rev s<sup>-1</sup>; ●, 10 rev s<sup>-1</sup>; ◆, 14 rev s<sup>-1</sup>; ▲, 18 rev s<sup>-1</sup>.

the different starting positions which occurred in the experiments. From this procedure, the mean and standard deviation of the cross-correlation function and of the peak time delay were determined.

Figure 12 shows the theoretical CPAS results of the chopper speed variation for an optically opaque sample ( $\tau_\beta = 10^{-4}$  s). A decrease of the peak magnitude with increasing rotation frequency is observed, with a peak delay time at  $\tau = 0$  s. The former observation is a trend qualitatively similar to the one observed experimentally with the Xerox toner (figure 8). The zero time delay is due to the large value of  $\beta$  chosen for the theory. For the large value of  $\beta$  chosen, the calculated pressure variation in the cell depends strongly on the surface temperature of the solid, whose variations follow the incident light intensity variations so closely (Mandelis and Royce 1979), that the cross correlation of

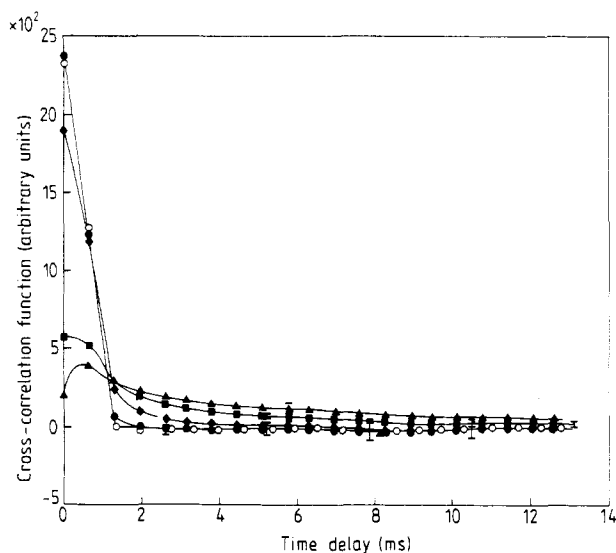


**Figure 13.** Theoretical CPAS signal showing the effects of  $\beta$  variation:  $\circ$ ,  $10^6 \text{ cm}^{-1}$ ;  $\bullet$ ,  $10^4 \text{ cm}^{-1}$ ;  $\blacklozenge$ ,  $10^3 \text{ cm}^{-1}$ ;  $\blacksquare$ ,  $10^2 \text{ cm}^{-1}$ ;  $\blacktriangle$ ,  $10 \text{ cm}^{-1}$ .

the input and output signals approximates the autocorrelation function of the input light intensity wavetrain. This function is known to peak at  $\tau = 0 \text{ s}$  for PRBS signals (Godfrey 1980). The cross-correlation function magnitude decreases with increasing chopper frequency, because a smaller amount of total optical energy is imparted to the material over one pseudo-period  $T$ . This is equivalent to the well-known signal amplitude decrease with increasing modulation frequency in F-D PAS (Rosenzweig and Gersho 1976). The error bars on the theoretical curves of figure 12 are due to the different starting positions along the PRBS sequence for the 20 cross correlations whose averages are shown in this figure.

Figure 13 shows numerical results of the effect of  $\beta$  variation on the CPAS theory. From this figure it can be seen that the cross-correlation function approximates a triangle function, i.e. an autocorrelation, for  $\beta \geq 10^4 \text{ cm}^{-1}$ . Furthermore, the time evolution of the correlation function becomes essentially independent of  $\beta$  for the same range of values, a phenomenon consistent with CPAS saturation. As  $\beta$  decreases, so does the CPAS magnitude, in qualitative agreement with our experimental results for  $\text{Ho}_2\text{O}_3$ , figure 10. The curve crossing of figure 13 is due to the fact that solids with smaller  $\beta$  contribute energy to the pressure wave, and therefore to the cross-correlation function, from deeper within the sample than those with higher  $\beta$ . The thermal energy of opaque spectral regions is essentially deposited at the surface and is conducted into the gas more rapidly than that of more transparent regions. Similar crossovers were observed experimentally (figure 10). Figure 13 also shows an increase in the peak time delay with decreasing  $\beta$ . The calculated values for this delay lie between 0 and 0.45 ms for the five CPAS curves shown.

Using the experimentally determined  $\alpha_s$  and  $\beta(\lambda)$  values, the theory was further applied to  $\text{Ho}_2\text{O}_3$ . The results of the theory are illustrated in figures 14 and 15. Comparison of figure 14 with figure 9 indicates that the theory predicts the experimental results well, but for the 'flyback' microphone effect and the absolute value of the peak

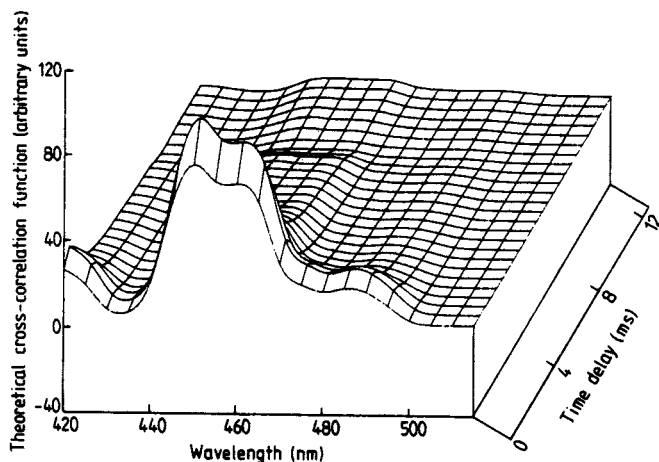


**Figure 14.** Theoretical cross-correlation function (CPAS spectrum) of normalised signal from  $\text{Ho}_2\text{O}_3$  powder. Chopper speed:  $6 \text{ rev s}^{-1}$ .

time delay. Figure 15 is also in general qualitative agreement with figure 10. The apparent discrepancy in the value of peak delay times between these two figures will be discussed below. The microphone 'flyback' effect, which is assumed to cause the crossing of the curves in figure 10, is also absent from figure 15.

Figure 16 shows a comparison between the CPAS peak magnitude obtained from  $\text{Ho}_2\text{O}_3$  experimentally at 8 nm resolution, and theoretically using our model with the calculated values of  $\alpha_s$  and  $\beta(\lambda)$ . The agreement is very good except for the highest  $\beta$  values, and indicates that the theory presented above can adequately describe the spectroscopic capabilities of CPAS. The departure of the theoretical curve from the data points at high  $\beta$ s has been attributed to the difference between the values of  $\beta$  used in

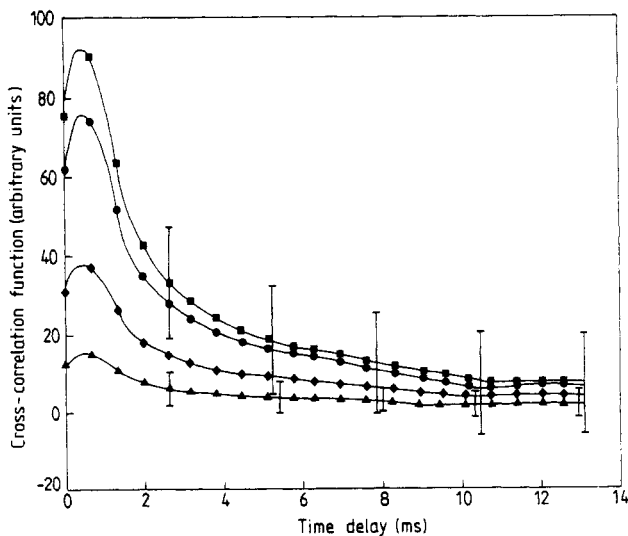


**Figure 15.** Theoretical cross-correlation function of  $\text{Ho}_2\text{O}_3$  at various wavelengths: ■, 450 nm; ●, 446 nm; ◆, 442 nm; ▲, 438 nm.

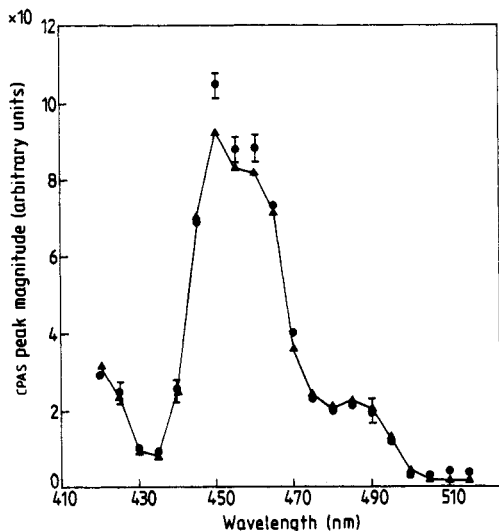


Figure 16. Wavelength dependence of the CPAS magnitude of  $\text{Ho}_2\text{O}_3$  at the peak delay time. —●—, experimental; —▲—, theoretical.

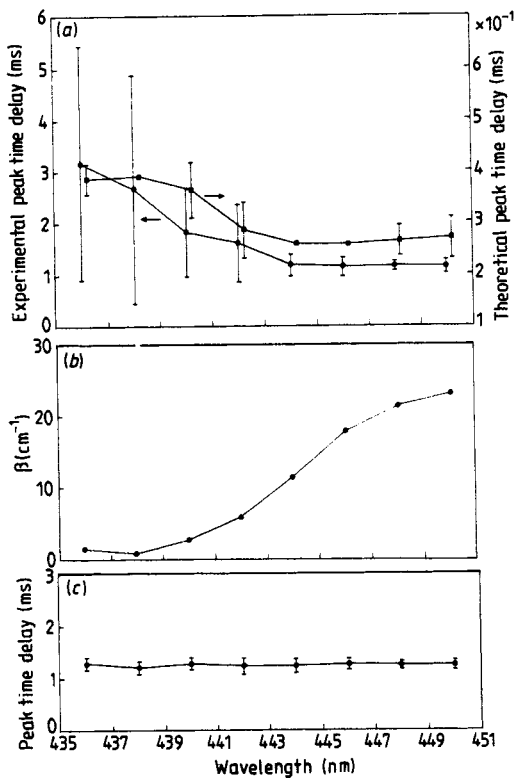


Figure 17. (a) CPAS average peak time delay for  $\text{Ho}_2\text{O}_3$ : theoretical and experimental curves. (b) Effective optical absorption spectrum of  $\text{Ho}_2\text{O}_3$  corresponding to (a) and calculated from F-D PAS spectra at 50 Hz modulation frequency. (c) CPAS average peak time delay for Xerox toner. Experimental curve.

the model in this rapidly varying spectral region and the actual  $\beta$  values, which our 8 nm resolution spectrometer could not accurately measure.

Figure 17(a) illustrates how the maximum time delay of the cross-correlation function changes with wavelength for both experiment and theory. Figure 17(b) is the optical absorption spectrum of  $\text{Ho}_2\text{O}_3$  powder from F-D PAS data corresponding to the same spectral region. Both theory and experiment show that as the optical absorption coefficient (and F-D PAS signal) decreases the peak time delay increases. This effect is consistent with the longer time delay  $\tau_\beta$  required for heat produced in the bulk to reach the sample surface at larger optical absorption depths. The varying time delay with  $\beta$  in CPAS can be thought to be analogous to the phase lag of the signal in conventional F-D PAS. The experimental results in figure 17(a) exhibit increased standard deviations in the optically transparent region below 443 nm due to the substantially decreased SNRS and the partial inability of the mathematical cross correlation to annihilate the noise component within one pseudo-period  $T$ . The trend for increasing time-delay mean values is very reproducible, however, and should be compared to the time delays observed for the photoacoustically saturated Xerox toner in figure 17(c). The opaque regions of  $\text{Ho}_2\text{O}_3$  have associated experimental peak time delays close to the (approximately) constant time delay  $\tau \approx 1.25$  ms of Xerox toner, as expected. While both theory and experiment are in reasonable agreement with respect to the change in peak time delay with absorption coefficient, the numerical values for the peak time delays between the two were found to differ substantially (figure 17(a)). This discrepancy is believed to be caused by the experimental apparatus itself, notably the roll-off in the microphone frequency response above approximately 10 kHz, which coincides with the earliest measurable cross-correlation times  $\tau$  in our experiments. A more complete, albeit more complex, theoretical approach would use equation (10), rather than its simplified version equation (11), in the response function formalism. Other sources of discrepancy most likely include the fact that the experimental PRBS optical wavetrain consisted of somewhat rounded, rather than square wave, pulses due to the finite spatial extent of the light sources used and especially the xenon lamp filament image. The effect of the frequency selection of the filter bandwidth  $\Delta\omega$  and the averaging time interval  $T$  were calculated assuming an ergodic random process with a relative fluctuation in the measurement  $z$ . The expression (Morrow 1958)

$$\sigma_z = E(z)/(\Delta\omega T)^{1/2} \quad (34)$$

was used, where  $E(z)$  is the mean value of the measurement and  $\sigma_z$  is the standard deviation. Further, it was assumed that the experimental PRBS was a stationary process (Godfrey 1980) with a gaussian first-order probability distribution; and the probability was calculated that  $z$  remains within  $\varepsilon$  of  $E(z)$  in 90% of all measurements (Crandall and Mark 1963):

$$\varepsilon = \sqrt{2}\sigma_z \text{erf}^{-1}(0.9) \quad (35)$$

$$= E(z)1.645/(\Delta\omega T)^{1/2}. \quad (36)$$

For  $T = 166.3$  ms and  $\Delta\omega = 2\pi(10^{-3}-30$  Hz), equation (36) yields  $\varepsilon/E(z) = 1.6\%$ . This result shows that, with 90% certainty that any isolated measurement would have an error of approximately 1.6%, our bandpass filtering effect at the pre-amplifier stage was small and, therefore, could not be the main cause for the peak time-delay discrepancy between experiment and theory. The oscillatory behaviour of the cross-correlation function at high chopper rotation frequencies shown in figure 8 is due to increased

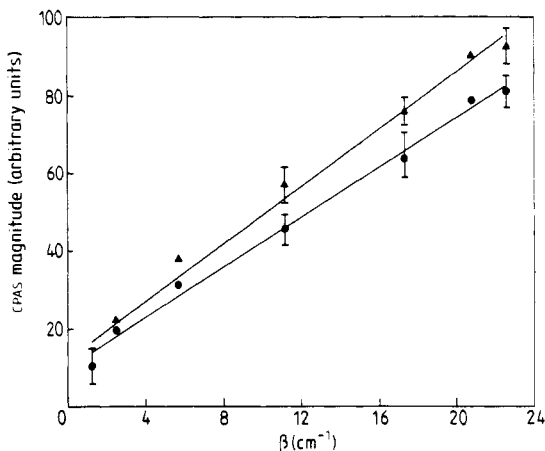


**Figure 18.** CPAS peak magnitude against optical absorption coefficient for  $\text{Ho}_2\text{O}_3$ : —●—, experiment; —▲—, theory.

wobbling of the chopper, since its centre of mass lies outside the rotation axis. In that case, a certain amount of energy is expected to be allotted to the periodic disturbance and will appear in the frequency spectrum of the chopper, as well as in the time domain of figure 8 as 'leakage' (Rota 1971). An effective way to greatly reduce the instrumental oscillations of figure 8 is to multiply the PRBS sequence  $F(t)$  with the Hanning window, if CPAS is to be used at high chopper rotation frequencies.

Within the optical absorption coefficient range of the investigated  $\text{Ho}_2\text{O}_3$  absorption band, the relationship between  $\beta(\lambda)$  and the experimental and theoretical peak magnitudes of the CPAS signal was found to be linear, figure 18. The agreement in both absolute values of the cross-correlation functions and in slopes is very good. Figure 18 shows that CPAS is a sensitive spectroscopic technique in the range of  $\beta$  values involved, and can be used quantitatively with the present theory to predict absolute values of  $\beta$ .

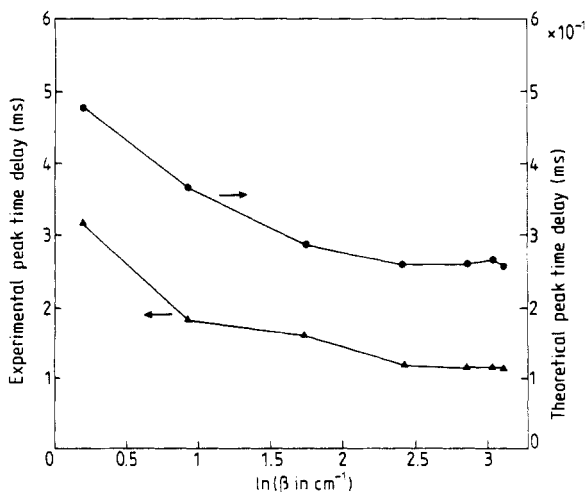


**Figure 19.** CPAS peak delay time variation with optical absorption coefficient for  $\text{Ho}_2\text{O}_3$ . —●—, experimental; —▲—, theoretical.

The linear dependence of CPAS magnitude on  $\beta$  is due to the fact that for the  $\beta$  values employed, the photoacoustic signal is far from saturation and can be shown to be proportional to  $\beta$  (Rosencwaig and Gersho 1976).

The CPAS peak time delay  $\tau_0$  does not bear a simple relation to  $\beta$ , either experimentally or theoretically. In general  $\tau_0$  increases as  $\beta$  decreases. The variation of  $\tau_0$  with the natural logarithm of  $\beta$  for the experimental and theoretical results can be seen in figure 19. Time delays corresponding to high absorption coefficients tend to limiting (saturation) values, with no apparent saturation of the respective magnitudes. These features are interesting and require further study before CPAS peak time delays can be used as a spectroscopic tool. Uejima *et al* (1984) have also found in general a mathematically complicated dependence of the peak time delay of the CPAS signal on the geometrical and thermal parameters of the sample in their model of a black absorber with a thin transparent surface layer.

## 7. Conclusions

Correlation photoacoustic spectroscopy has been shown experimentally and theoretically to be a photothermal technique sensitive to spectroscopic parameters in solids and capable of performing quantitative spectroscopic measurements. Our results indicate that for values of the optical absorption coefficient above approximately  $0.5 \text{ cm}^{-1}$ , the cross-correlation function peak magnitude is linearly related to  $\beta$ , while the peak time delay is related to  $\beta$  in a more complicated fashion. The proposed one-dimensional theoretical model exhibits parameter dependences in agreement with the experimental evidence, with certain absolute value discrepancies presumably due to instrumental factors which were not accounted for in the model. It appears that the poor SNR is a limiting factor toward the use of CPAS as a spectroscopic technique with transparent samples ( $\beta \leq 5 \text{ cm}^{-1}$ ). Photoacoustic saturation is expected to be the main limiting factor for  $\beta \geq 10^3 \text{ cm}^{-1}$ , in agreement with conventional PAS theory. The promise of CPAS to yield high SNRs at high frequencies due to its impulse-response equivalence and its claimed SNR superiority to pulsed time-domain PAS (Kirkbright and Miller 1983) may conceivably extend the range of high  $\beta$ s accurately measurable by photoacoustic spectroscopic techniques. The present work indicates, however, that the transducer frequency response is a major factor limiting this range when microphone-gas-coupled CPAS is employed.

## Acknowledgments

The authors wish to acknowledge the financial support of the National Science and Engineering Research Council of Canada (NSERC) throughout this research. We are also grateful to Dr Y Hassan, Department of Mechanical Engineering, University of Toronto, for many interesting and enlightening discussions and comments on the manuscript.

## References

- Adams M J and Kirkbright G F 1977a *Analyst* **102** 281

- 1977b *Analyst* **102** 678
- 1976 *Spectrosc. Lett.* **9** 255
- Carlson K D and Hodul D 1982 *J. Photoacoust.* **1** 291
- Cox M F and Coleman G N 1981 *Anal. Chem.* **53** 2034
- Crandall S H and Mark W D 1963 *Random Vibration in Mechanical Systems* (New York: Academic) ch 1
- Gemlin L 1974 *Handbuch der Anorganischen Chemie*, vol. 39 (Heidelberg: Springer) p 141
- Godfrey K R 1980 *Automatica* **16** 527
- Golomb S W 1967 *Shift Register Sequence* (San Francisco: Holden Day)
- Hass G, Ramsay J B and Thun R 1959 *J. Opt. Soc. Am.* **49** 116
- Kato K, Ishino S and Sugitani Y 1980 *Chem. Lett. Chem. Soc. Japan* 783
- Kirkbright G F and Miller R M 1983 *Anal. Chem.* **55** 502
- Kirkbright G F, Miller R M and Rzadkiewicz A 1983a *J. Physique* **10** C6 249
- Kirkbright G F, Miller R M, Spillane D E M and Sugitani Y 1984a *Anal. Chem.* **56** 2043
- Kirkbright G F, Miller R M, Spillane D E M and Vickery I P 1983b *J. Physique* **10** C6-243
- 1984b *Analyst* **109** 1443
- Mandelis A and Royce B S H 1979 *J. Appl. Phys.* **50** 4330
- 1980 *J. Appl. Phys.* **51** 610
- Mandelis A, Siu E and Ho S 1984 *Appl. Phys. A* **33** 153
- Mandelis A, Teng Y C and Royce B S H 1979 *J. Appl. Phys.* **50** 7138
- Morrow C T 1958 *J. Acoust. Soc. Am.* **30** 456
- Rosencwaig A and Gersho A 1976 *J. Appl. Phys.* **47** 64
- Rota P R 1971 *IEEE Spectrum* **70** 50
- Schoonover J R, Yng-Long Lee, Su S N, Lin S H and Eyring L 1984 *Appl. Spectrosc.* **38** 154
- Spiegel M R 1965 *Theory and Problems of Laplace Transforms* (New York: McGraw-Hill)
- Sugitani Y and Uegima A 1984 *Bull. Chem. Soc. Japan* **57** 2023
- Sugitani Y, Uegima A and Kato K 1982 *J. Photoacoust.* **1** 217
- Tilgner R 1981 *Appl. Opt.* **20** 3780
- Uejima A, Curtis D and Sugitani Y 1984 *J. Photoacoust.* **1** 397
- Uejima A, Sugitani Y and Nagashima K 1985 *Anal. Sciences* **1** 5